International Journal of
Innovation in Mechanical Engineering & Advanced Materials (IJIMEAM)
https://publikasi.mercubuana.ac.id/index.php/ijimeam

Vol.5 (No.1). 2023. pp. 16-25
Published online: April 1, 2023
ISSN: 2477-541X

COMPARISON OF THE DRYER AIR INLET POSITION ON THE SPRAY DRYER WITH A DOUBLE CONDENSER TO PRODUCE A ROTATING FLOW THROUGHOUT THE DRYING CHAMBER: CFD ANALYSIS

*Nanang Ruhyat**

Department of Mechanical Engineering, Universitas Mercu Buana, Meruya Selatan, Jakarta 11650, INDONESIA

Abstract

Simulation of the drying air and the spray of liquid in the spray dryer chamber with Discrete Phase Material (DPM) and Discrete Random Walk (DRW) was presented in this study using CFD methods to analyze the drying liquid. The main problem in spray drying is the adhesion of the material to the drying chamber walls, which causes uneven drying material. This adhesion can slow down the drying process and reduce productivity. The design of the drying air inlet into the drying chamber becomes essential to research. Variations in the position of the drying air inlet into the drying chamber are carried out in the 3D spray dryer room to see the mechanism of the centrifugal velocity of the drying airflow, which can improve uniform mixing with flow resistance due to friction with small walls and the drying air velocity. This phenomenon is impossible to observe in experiments. A geometric model consisting of 1,054,000 hexa-mesh elements at the area around the nozzle, the top spot of the chamber and the remaining area covered with a tetrahedral mesh, was determined to predict velocity, temperature, and fluid flow behavior. The first position, the dryer air inlet, is at an angle from the diameter of the spray drying chamber. The second position is in the middle of the diameter of the drying chamber. The position of the first inlet produces a more even temperature contour with a more tangential velocity due to the small frictional resistance with the walls. At the same time, the second position is not recommended because the flow leads to one side of the wall and creates sticking and even material buildup. A double-heated condenser can dry air at moderate temperatures, and it is a very effective drying product—positioning the dryer air inlet into the drying chamber, achieving the economical production of high-quality products.

Keywords: Dry Air Inlet, Drying Process Material, Discrete Random Walk, CFD, Spray-Dryer

*Corresponding author: Tel. +62 21 5840815 Ext. 5200
E-mail address: nanang.ruhyat@mercubuana.ac.id

DOI: 10.22441/ijimeam.v5i1.21605

1. Introduction

Spray-dryers have been known since 1870. Spray-dryers are generally used in the pharmaceutical, chemical, and food industries for drying[1]. The dryer changes the liquid phase of the material to be dried with drying air[2] into a vapor phase and then removes water vapor in the liquid material to become dry powder[3]. Dryers can reduce or eliminate microbial growth on the material by reducing the water content[4].

Several things that the researcher did before in determining dryer product quality as inlet drying temperature[5–7], feed flow rate[8], ambient temperature and relative humidity[9], Feed Concentrated [9], Atomization speed[6, 10–12], Inlet air velocity and pressure operation as well as outlet temperature[13], and droplet diameter[14].

In addition to the seventh thing above, it can also be done by constructing the drying air inlet hole connected to the drying chamber to increase the effect of swirling flow in the material drying chamber.

The practical structure of the air-liquid junction mechanism, which is more efficient in producing dry powder, is urgently needed and has yet to be studied. Measurement of airflow, temperature, particle size, and humidity in the drying chamber is challenging and expensive to perform in large-scale dryers.

Previously, researchers had conducted experiments with double condensers from the refrigeration system[3]. The humidity of the air that will enter the heater room has been successfully reduced to increase the quantity of the product. Understanding particle collisions in the drying chamber is essential to study because it affects the quality of the final product.

A 3D CFD model of the agglomeration of

Vol.5 (No.1). 2023. pp. 16-25
Published online: April 1, 2023
ISSN: 2477-541X

droplets and particles in a counter-current spray-drying process has been studied[15]. Experimental numerical methods in kinetic drying show similar results[16]. The CFD is software that can predict drying phenomena in numerical analysis, as many researchers have done[1, 3]. For turbulent and economical model analysis, CFD analysis with k-ε is used[14], while to predict a more accurate flow field in the spray dryer process, the RSM method is used[15, 16]. Discrete Phase Material (DPM) is a model of material particles in the form of a ball, as a droplet or bubble followed by a type of impact, as Discrete Random Walk (DRW) methods that will occur between the material particles and the walls designed in the simulation.

In order to increase the efficiency of the drying process in the drying chamber, the effect of the position of the drying air inlet in the drying chamber will be investigated. Spray drying converts liquid food into a dry particulate form by spraying the food material into a hot drying medium. It provides an overview of the spray dryer machine with heating from the heater and exhaust heat from the condenser in the refrigeration system. The spray dryer machine, with a combination of heating from the heater and exhaust heat from the condenser in the refrigeration system, has answered concerns about the effect of high ambient air humidity when drying materials. Dry air with low humidity can increase the flow rate of compressed air. Increasing the drying airflow rate in the drying chamber can reduce the mean spray droplet size[15]. This method is better than shrinking smaller particles. As the particles shrink, a narrower spray cone is formed, and air may not penetrate the center of the spray pattern until the droplet has traveled a considerable distance from the nozzle. In addition, it reduces the mixing of the material with the hot air, thereby reducing the drying rate.

Although modifications to the spray dryer as described above have been made, the quality of the product is greatly influenced by the drying conditions. The thermal damage to the product during direct drying is highly proportional to the drying temperature and the residence time of the particles in the drying chamber. In addition, droplets and dry powder adhere to the dryer wall due to the sugar-drying solution[7]. Adhesion and subsequent deposition of the material on the dryer's surface are still considered severe problems encountered in industrial spray drying.

Various means of dealing with such products have been investigated over the years, such as the addition of a drying aid (maltodextrin), cooling the walls of the drying chamber, and the entry of atmospheric air near the bottom section, enabling the transport of powder to a collector that has atmospheric humidity. Masters et al. modified the jacketed wall for air conditioning, but it caused an increase in the relative humidity of the air close to the wall surface[8].

The drying chamber's airflow, temperature, particle size, and humidity measurement is tough and expensive to perform in large-scale dryers. CFD can be a helpful tool for predicting gas flow patterns and particle phenomena such as temperature, velocity, residence time, and collision position with 3D images. CFD modeling has been widely used for drying processes to study heat and mass transfer[7] simultaneously. Although the simulation of complex transport phenomena occurring in the spray dryer cannot be modeled with high accuracy, the results are still helpful in guiding the design and operation of the spray dryer when combined with empirical experience. CFD method to investigate airflow patterns, temperature, and humidity profiles at various positions in the spray drying chamber. It should be noted that the drying process is controlled by two critical factors: the convection heat transfer coefficient, which is directly related to the air velocity, and the residence time in the drying chamber[19].

Previous research[2] has shown how the product quantity is increased by accelerating the drying air flow rate and how the product does not stick to the wall by maintaining the relative humidity along the outer wall of the drying chamber. However, there is an unresolved problem related to the tangential velocity of the drying air in the drying chamber, which can result in a more uniform flow throughout the drying chamber and a longer residence time for the particles to mix with the liquid material in the drying chamber.

This study focuses more on the results of the drying simulation in the drying chamber, where two variations of the inlet from the drying air to the drying chamber are made. The effect of the inlet position was analyzed and discussed in order to minimize friction with the drying chamber walls. The results can be seen in the 3D view of the drying chamber to investigate which parts can reduce the number of material particles attached to the wall as expected before the experimental step is conducted.

The study aims to get a better effect on the positions of the drying air inlet in the drying chamber. For this reason, the following objectives are accomplished; (1) Comparing the position of the drying air inlet into the drying chamber from variations that can create airflow with a more incredible tangential velocity of rotating dryer airflow, (2) Analyzing temperature distribution

Vol.5 (No.1). 2023. pp. 16-25
Published online: April 1, 2023
ISSN: 2477-541X

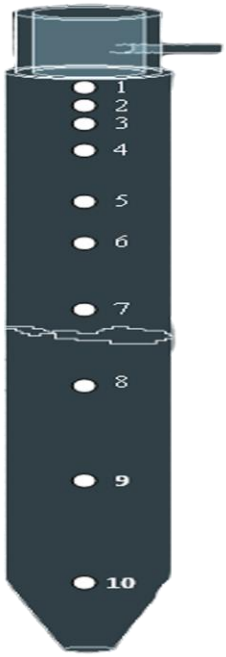

Fig. 1. Geometry mesh in the Drying Chamber

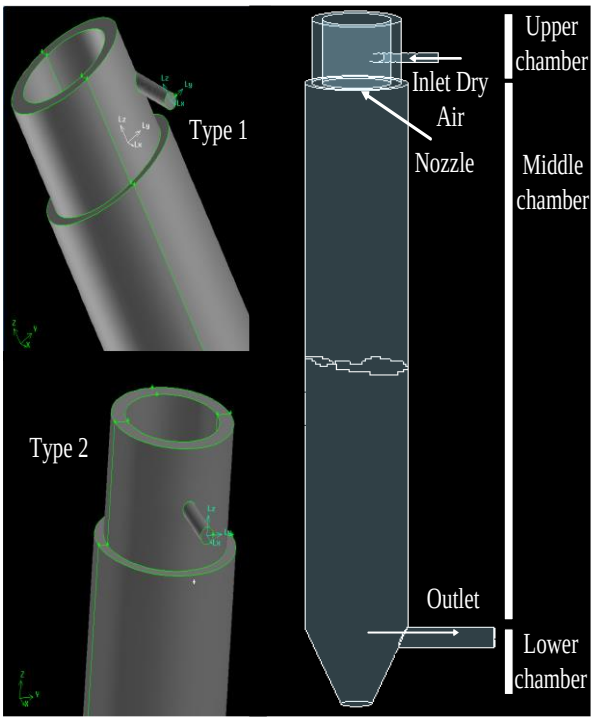

Fig. 2. Geometry model from the drying chamber

between inlet position variations.

2. Numerical Simulation and Procedures

2.1 Initial Data for Simulation

In the early stages of the simulation, the meshing process must be done after the image is created. The mesh must cover the spray dryer drying chamber's top, bottom, and middle with the appropriate netting quality. This simulation was conducted at a constant temperature and flow rate of 60 °C and 0.003 kg/s, respectively. The temperature of 60 °C is set because it is the lowest temperature representing a safe temperature for drying food or heat-sensitive materials.

The measuring point placement in the drying chamber is distributed in 10 simulation points, as shown in Fig. 1. Fig. 1 and Table 1 show the position of the temperature nodes to describe the temperature distribution in the y-direction. The node's role is described in Table 1, where the coordinate center is at the nozzle position. The positions of node 1–4 were deliberately arranged close to each other and close to the chamber entrance to capture the quality of the mixture between dry air and spray nozzle.

The geometric model for numerical analysis is shown in Fig. 2. The variation of the position of the drying air inlet in the drying chamber shows variations 1 and 2 at the top and bottom of Fig. 2. It shows the 3D space of the spray dryer, where the droplets interact with the air dryer. Overall, the geometry consists of 1,054,000 elements. However, not all chamber areas are covered with the same mesh type. Some places should be covered with hex mesh, especially around the nozzle and the chamber's top spot. All areas will be covered with a tetrahedral mesh.

Furthermore, Fig. 2 shows two types of the position of the air duct that enters the drying chamber, namely type 1, with an inlet from the side of the drying chamber, and type 2, which is a channel that enters from the center of the drying chamber.

2.2 The Governing Equation of The Continuous Phase

By ignoring the time-derived term, the governing equation forms an energy storage term—the net rate of energy entering by convection.
Continuity equation:

$$\frac{\partial \rho u_i}{\partial x_i} = M_m \tag{1}$$

Table 1. Node position of temperature in y direction

Node	*Y* (m)	Node	*Y* (m)
1	–0.02	6	–0.14
2	–0.03	7	–0.2
3	–0.06	8	–0.3
4	–0.08	9	–0.4
5	–0.12	10	–0.86

Vol.5 (No.1). 2023. pp. 16-25
Published online: April 1, 2023
ISSN: 2477-541X

Momentum equation:

$$\frac{\partial \rho u_i u_j}{\partial x_i} = \frac{-\partial}{\partial x_j} + \frac{\partial}{\partial x_i} X \left[\mu \left(\frac{\partial y}{\partial x} + \frac{\partial y}{\partial x} \right) - \rho \overline{u_i' u_j'} \right] + M_f \quad (2)$$

Energy Equation:

$$\frac{\partial \left(\rho C_p u_j T \right)}{\partial x_i} = \frac{\partial}{\partial x} \left[k \frac{\partial T}{\partial x_i} - \rho \overline{u_i' T'} \right] + M_h \quad (3)$$

Heat conduction flows in the fluid at a specified distance so that the temperature control of the space can be seen in particle momentum velocity. The value of k is the effective conductivity, and T is the temperature.

The CFD code solves a system of partial differential equations with the approach taken for droplets as particles called the discrete phase model. DPM in CFD code will capture the interaction between continuous and discrete phases. Since two phases were simulated in the software, continuous and discrete, the governing equation will be explained hereafter[19].

2. 3 The Governing Equation of The Discrete Phase

The Euler-Lagrange governing eq. for the trajectory of the particle to solves the balance of forces on the particle expressed as follows [19]:

$$\frac{\partial u_{pi}}{\partial x_i} = C_d \frac{18 \mu R_e}{\rho_p d_p 24} \left(u_i - u_{pi} \right) + g_i \frac{\rho_g - \rho}{\rho_g} + F_{xi} \quad (4)$$

The standard *k–ε* model uses a wall function to describe the effect of the wall (the relationship between Reynolds stress and mean velocity gradient and turbulent viscosity) on the average flow (turbulent range) and shifts to a low Reynolds number formulation at low *Re*. The standard *k–ε* model can improve the accuracy of rotating flow fast-flowing tension and can also handle the problem of low Re quite well.

2. 4 Mass and Heat Transfer Between Two Phases

The evaporation rate between the particles and the hot air can be seen in the diffusion gradient in eq. (5) and can be seen as follows[19]:

$$N_i = k_c \left(C_{i,s} - C_{i,\infty} \right) \quad (5)$$

The heat transfer between droplets and hot air can be represented as follows:

$$m_\rho C_\rho \frac{dT_p}{dt} = hA_p \left(T_\infty - T_p \right) + \frac{dm_p}{dt} h_{fg} \quad (6)$$

Several studies provide prominent comments on the use of the turbulent model. Compared to the RSM and k-ε model, using *k-ε* is more economical and makes more sense. Because the model gives a slight difference in the results regarding speed, temperature, and mole fraction[19], this simulation uses a realizable k-ε turbulent model based on ANSYS in the following. While for equation *k*, expressed as follow.

$$\frac{\partial \rho k}{\partial t} + \frac{\partial \rho k u_j}{\partial x_j} = \frac{\partial}{\partial x} \left[\left(\mu + \frac{\mu_t}{\mu_k} \right) \frac{\partial k}{\partial x_j} \right] + G_k + G_b - \rho \varepsilon - Y_m + S_k \quad (7)$$

G_k and G_b are the kinetic energy of the velocity gradient and buoyancy, respectively[3]. The contribution of dilatation fluctuations incompressible turbulence to the overall dissipation rate is Y_m. S_k and S_ε are source terms. Thus, ε equation expressed as;

$$\frac{\partial \rho \varepsilon}{\partial t} + \frac{\partial \rho \varepsilon u_j}{\partial x_j} = \frac{\partial}{\partial x} \left[\left(\mu + \frac{\mu_t}{\mu_g} \right) \right] + \rho C_1 - \rho C_1 \frac{\varepsilon^2}{k + \sqrt{v\varepsilon}} + C_{1\varepsilon} \frac{\varepsilon}{k} + C_{1\varepsilon} \frac{\varepsilon}{k} C_{1\varepsilon} G_b + S_\varepsilon \quad (8)$$

$$C_1 = max \left[0.43 \frac{\eta}{\eta + 5} \right], \ \eta = S \frac{k}{\varepsilon}, \ s = \sqrt{2 S_{ij} S_{ij}} \quad (9)$$

The value $C_{1\varepsilon}$ and $C_{3\varepsilon}$ is a constant defined in ANSYS FLUENT. One of the salient features of the k-ε realizable model is that the production of *k* does not involve, so the terms G_k are not the same. The difference between the standard *k-ε* and *k-ε* realized models is the destruction term (second term on the right) in equation (8). The denominator of the destruction term is never zero, but the value of *k* is minimal. The realizable *k-ε* model is better than the *k-ε* attainable model for all the cases.

Simulations were carried out under steady conditions. The turbulent model is realizable *k-ε*, using DPM (Discrete Phase Model) and DRW (Discrete Random Walk) to capture the interaction between continuous and discrete phases. The speed-pressure coupling scheme in this simulation is simple. There are several assumptions involved, including the chamber wall is adiabatic, so there is no energy transfer between the wall and the environment, the friction between the droplets and the wall is relatively small, and the distribution of the spray dryer on the nozzle using a Rosin-Rammler distribution[18–19].

The DRW Model is a method to predict particle trajectories based on statistics. This calculation uses a stochastic approach that can be run based on the

Vol.5 (No.1). 2023. pp. 16-25
Published online: April 1, 2023
ISSN: 2477-541X

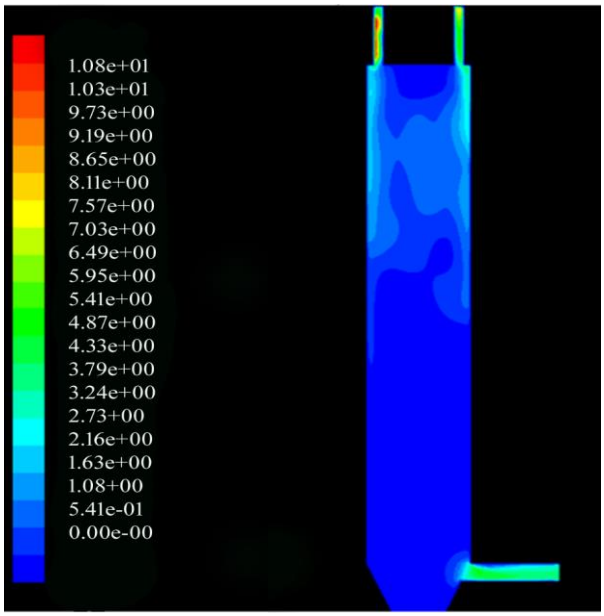

(a)

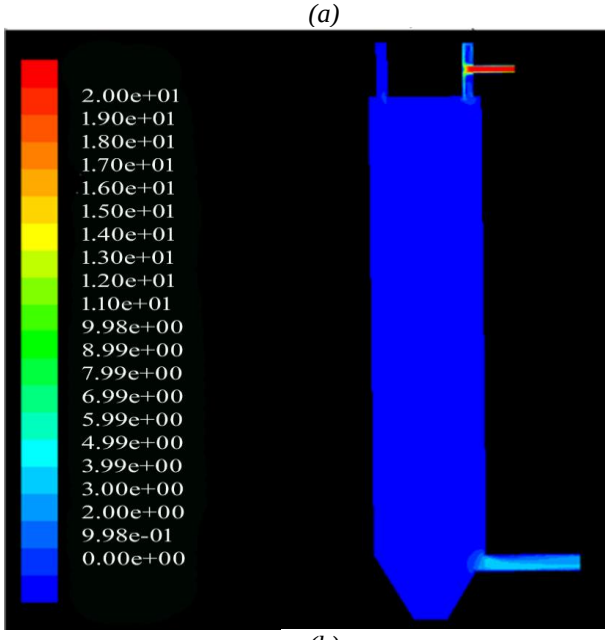

(b)

Fig. 3. Velocity contour at axial position: (a) inlet from the side of the drying chamber; (b) duct entering from the center of the drying chamber

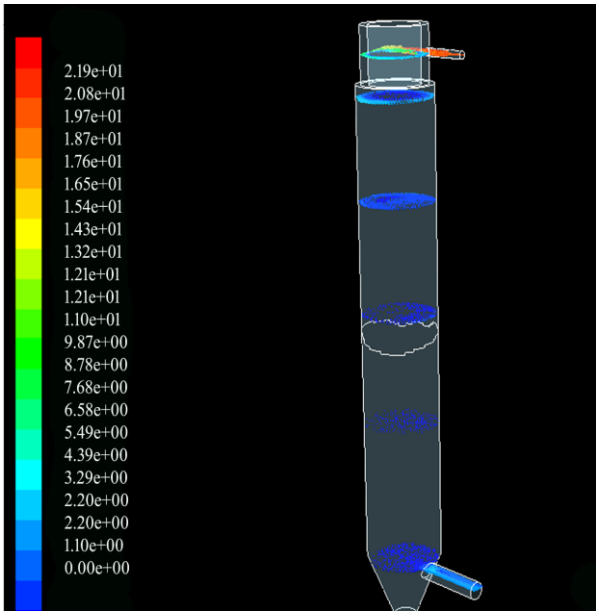

(a)

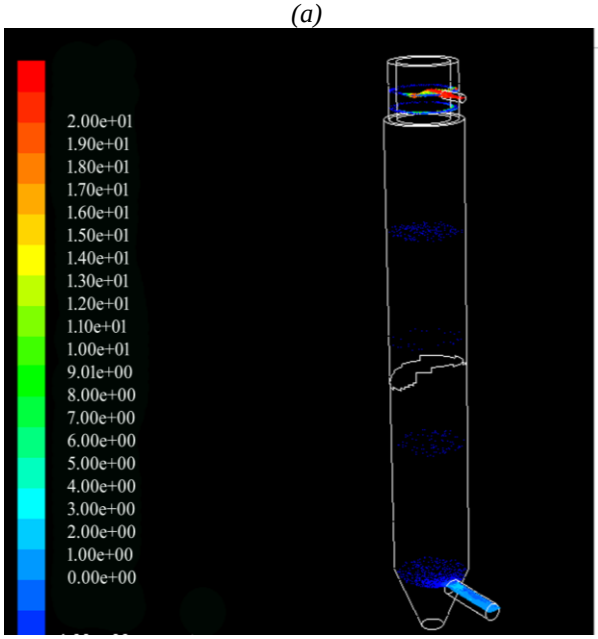

(b)

Fig. 4. Velocity vector inside spray dryer in radial position: (a) inlet from the side of the drying chamber; (b) inlet from the center of the drying chamber

number of definitions in the simulation. Generally, the DRW formula is given in equation (10) in the form of integral of time.

$$T = \int_0^{\infty} \frac{u'_p(t)\, u'_p(t-\tau)}{\overline{u'^2_p}} d\tau \qquad (10)$$

Equation (10) shows a proportional relationship between particle dispersion because the greater the value of T, the greater the flow turbulence. When the particle tracer is on a small scale, the equation will turn into a time integral as follows:

$$T_L = C_L \frac{k}{\varepsilon} \quad (11) \qquad (11)$$

$$T_L \approx 0.3 \frac{k}{\varepsilon} \quad (12) \qquad (12)$$

The C_L value will be determined in a turbulent model, such as using the k-ε model. The computational model considered is standard k–ε model. The resolution of the mesh around the wall depends on the model used in the simulation.

Vol.5 (No.1). 2023. pp. 16-25
Published online: April 1, 2023
ISSN: 2477-541X

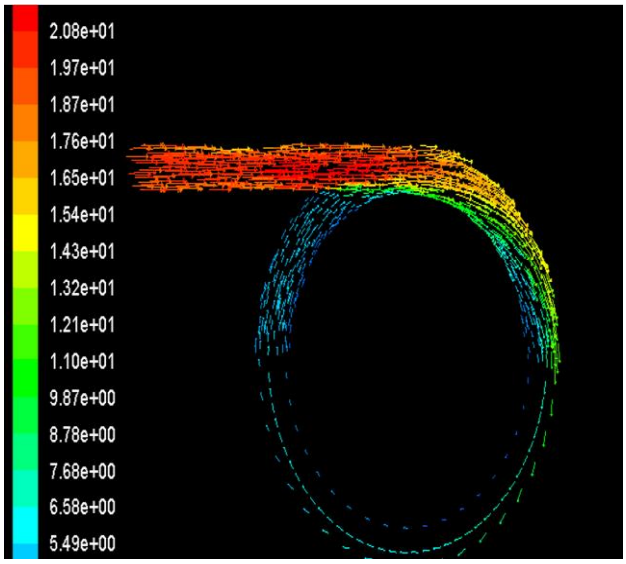

(a)

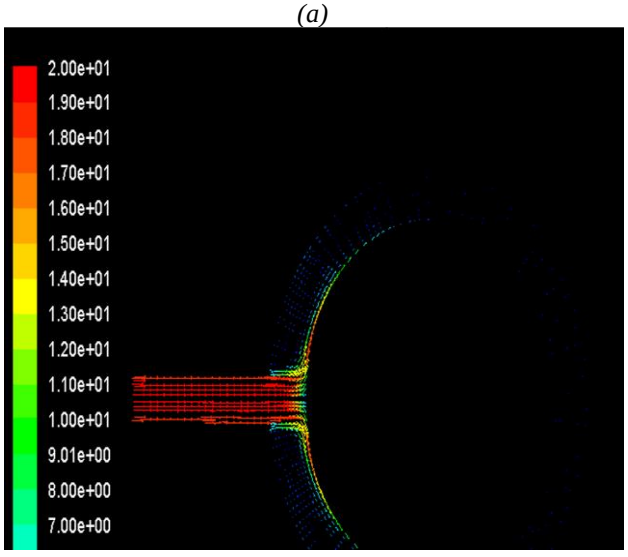

(b)

Fig. 5. Comparison of the velocity vector at z=0.05 in radial position: (a) inlet from the side of the drying chamber;(b) inlet from the center of the drying chamber

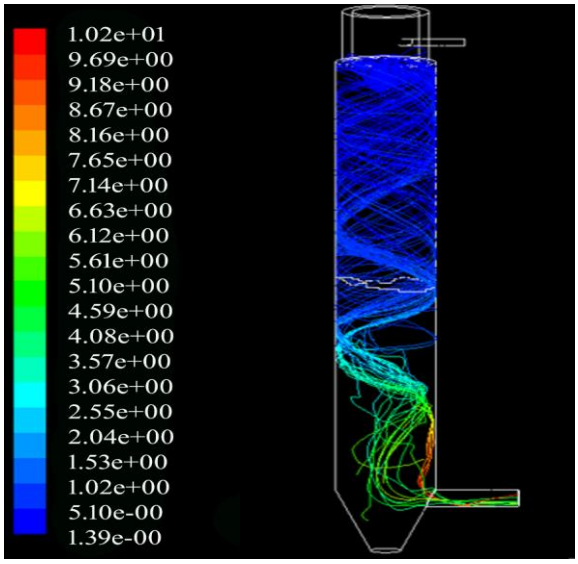

(a)

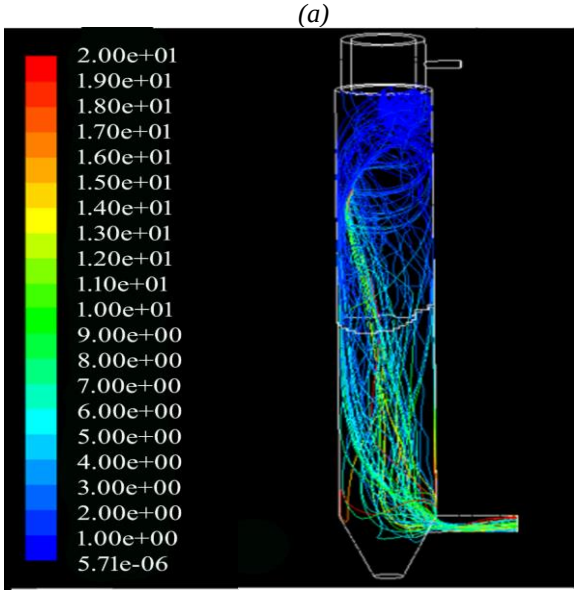

(b)

Fig. 6. Comparison of particle track in variation 1 and 2; (a) inlet from the side of the drying chamber, (b) inlet from the center of the drying chamber

3. Results and Discussion

3.1 Numerical Results of Inlet Position Effect on Drying Quality

The results of the study were discussed separately in two parts, which show the difference in the quality of tangential velocity and temperature distribution. These two values are indicators that the drying carried out shows some results that show quality improvement in the drying effect.

3.2 Tangential Velocity

From the simulation, tangential velocity results show the effect of positioning the drying air inlet into the drying chamber to airflow with a more incredible tangential velocity of rotating dryer airflow. The velocity contours of the axial plane variations 1 and 2 are shown in Fig. 4. The air velocity of the dryer and the spray nozzle initially has a significant effect near the inlet. It gradually decreases as it gets further away from the inlet due to pressure loss and friction near the wall. In variation 2, the decrease in speed is more significant than in variation 1. The velocity at the center line was lower because it had more excellent resistance. That is, variation 2 has a greater resistance in the axial position. The resistance of variation 2 arises from friction of the walls and the collision of dry air with the middle wall in the upper chamber.

In Fig. 3, the velocity contour at variation 2 is more homogenous than variation 1. The tangential velocity faded at the outlet due to pressure loss and friction near the wall. Fig. 5 shows the tangential

Vol.5 (No.1). 2023. pp. 16-25
Published online: April 1, 2023
ISSN: 2477-541X

velocity in the drying chamber with the same result as Fig. 3. The tangential velocity will fade at the outlet due to pressure loss and friction near the wall. A comparison of the tangential velocity vectors between variations 1 and 2 at the same height shows that the vector in variation 1 is more significant than in variation 2. This tangential velocity causes the dry air to reach the diameter of the drying chamber and produces a rotating flow throughout the drying chamber. Variation 1 has a more significant vortex motion than variation 2, as shown in the particle's trajectory.

A comparison of the tangential velocity vectors between variations 1 and 2 at the same height shows that the vector in variation 1 is more significant than in variation 2. This tangential velocity causes the dry air to reach the diameter of the drying chamber and produces a rotating flow throughout the drying chamber.

It can be seen in Fig. 4 that both variations 1 and 2 have secondary flows. The secondary flow in variation 1 is visible after the dry air has fully reached the upper chamber's circular path. Whereas in variation 2, secondary flow only appears near the inlet due to the collision of dry air against the middle wall. In variation 2, adjacent streams were pulled by an imaginary force that tended to lean to the right of the chamber.

Fig. 5 shows a comparison of variations 1 and 2 in the trajectory of the spray nozzle particles. In variation 1, it is seen that the trajectory of the spray nozzle particles has a more significant circular motion than variation two because the tangential velocity is as described in Fig. 6. Therefore, it will increase the mixing process between the drying air and liquid material, and the residence time of the particles becomes longer. While variation 2, it has a smaller tangential velocity than variation 1, thus reducing the circular motion. Consequently, the quantity of drying products is less, and the residence time will be faster.

Fig. 6 shows a comparison of variations 1 and 2 in the trajectory of the spray nozzle particles. In variation 1, it is seen that the trajectory of the spray nozzle particles has a more significant circular motion than variation two because the tangential velocity is as described in Fig. 5. Therefore, it will increase the mixing process between the drying air and liquid material, and the residence time of the particles becomes longer. While variation 2, it has a smaller tangential velocity than variation 1, thus reducing the circular motion. Consequently, the quantity of drying products is less, and the residence time will be faster.

3.3. Temperature Distribution

The temperature distribution with different inlet orientations is shown in Fig. 8. Variation 1 has a more uniform temperature than variation two due to less inhibition in the axial direction and more significant circular motion. A minor inhibition in variation 1 will have a more incredible axial velocity and circular motion, which supports the mixing process between dry air and nozzle spray.

Meanwhile, the temperature contour of variation 2 is not uniform because of the dry air resistance in the axial position and the small circular motion. The effect is on the uneven mixing process. In addition, the impact of the collision between dry air and the middle wall in variation 2, apart from being a flow blocker, appears as secondary flow near the inlet, which tends to point to the right side of the drying chamber.

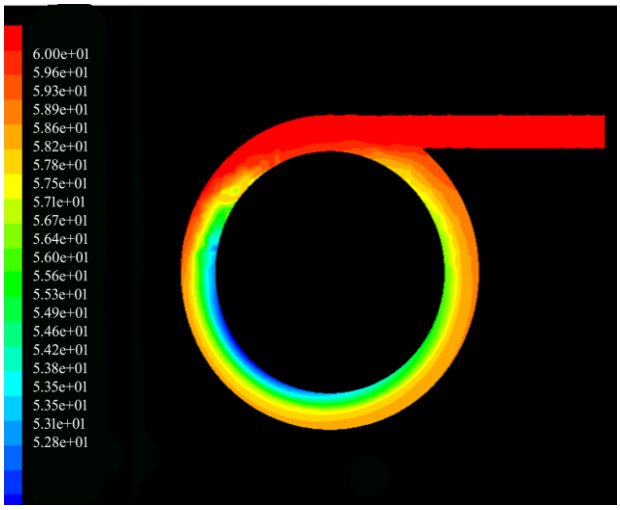

(a)

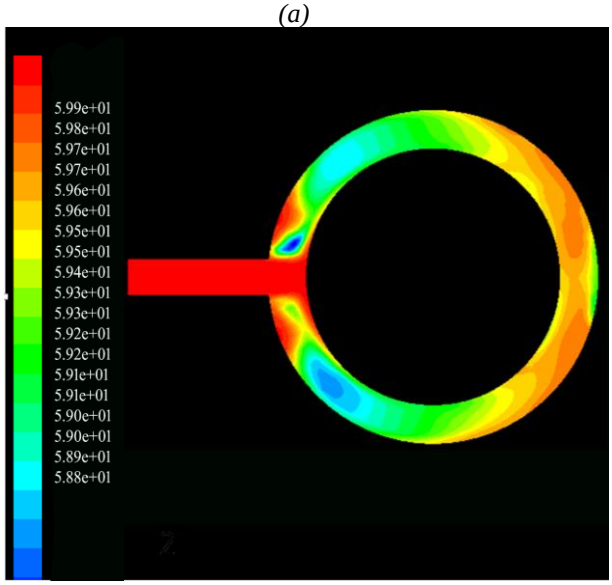

(b)

Fig. 7. Comparison of radial temperature contour between variation 1 and 2; (a) inlet from the side of the dry room, (b) inlet from the center of the drying chamber

Vol.5 (No.1). 2023. pp. 16-25
Published online: April 1, 2023
ISSN: 2477-541X

Fig. 7 shows the radial temperature in the upper chamber. It is shown that a more incredible tangential velocity will make the radial temperature more uniform because this velocity supports dry air to flow along a circular path and reach the entire diameter of the spray drying chamber, as described in Fig. 8. This evidence will answer why the radial variation of contour 2 is not uniform. It shows that the tangential velocity significantly affects the mixing process at the radial position.

Furthermore, Fig. 8 in the graph shows how the temperature distribution in the drying chamber is. The comparison of the chamber temperature distribution along the y-direction between variations 1 and 2 is shown in Fig. 8. This indicates that temperature variation 1 increased significantly than variation 2. It implies that the mixture quality between the spray nozzle and the dry air is well mixed. However, getting further away from the heat source, temperature variations 1 and 2 lead to the same pattern: a decrease in temperature at node 10.

3.4. Discussion of Experimental Results of Effect of Inlet Position on Drying Quality

The position of the inlet in variation 2 could be more efficient, where the inlet in the middle provides a significant flow resistance. The radial velocity image shows that the flow resistance in variation 1 is smaller than in variation 2. So, it has a better radial velocity than variation 2. As a result, variation 1 has better mixing. As seen in Fig. 4. The velocity contours of the two positions initially have a significant effect. Significant near the inlet. However, it gradually decreases because it is further away from the inlet, and the pressure decreases. Besides that, friction occurs near the walls of the drying chamber. In variation 2, the decrease in speed is more significant than in variation 1. Variation 2 has a more significant resistance in the axial position. The resistance of variation 2 arises from the friction of the walls and the collision of dry air with the middle wall from the upper room. Fig. 5. shows the tangential velocity will fade at the outlet due to pressure loss and friction near the wall. The comparison of the tangential velocity vector between variations 1 and 2 at the same height shows that the velocity vector in variation 1 is more significant than in variation 2. This tangential velocity produces a rotating flow throughout the drying chamber. Variation 1 has a more substantial vortex motion than variation 2. This motion had been seen in the trajectory of the particle.

In Fig. 6, both variations have secondary flows. The secondary flow in variation 1 is visible after the dry air has completely reached the circular path in the upper chamber. Whereas in variation 2, secondary flow only appears near the inlet due to the collision of dry air against the middle wall. In variation 2, adjacent streams are pulled by an imaginary force to tend to lean to the right side of the chamber, as shown in Fig. 8. This illustrates that the product will accumulate on the right side of the drying chamber.

Fig. 8 shows a comparison of variations 1 and 2 in the trajectory of the spray nozzle particles. In variation 1, it shows that the trajectory of the spray nozzle particles has a more significant circular motion than the second variation. The increase in the tangential velocity of the intake air increases the velocity increase due to the increase in residence time. The increase in the evaporation rate in the drying chamber is due to the particle trajectory following the airflow, which has a tangential velocity, so larger particles remain, which means faster evaporation time. Meanwhile, variation 2 has a smaller tangential velocity than variation 1, reducing circular motion. As a result, the drying product is less, and the residence time will be faster.

A more uniform temperature contour is seen in variation 1 than in variation 2 in Fig. 8. Smaller resistance in the axial direction and a more significant circular motion are shown in variation 1. Axial velocity and circular motion are more remarkable in variation 1, favoring the mixing process between dry air and a more even nozzle spray.

The temperature contour of variation 2 is not uniform because of the dry air resistance in the axial position and small circular motion. The effect is on the uneven mixing process. It indicates that the tangential velocity significantly affects the mixing process at the radial position. In addition, the impact of the collision between dry air and the middle wall in variation 2 other than as a flow blocker, the secondary flow appears near the inlet, which tends to lead to the

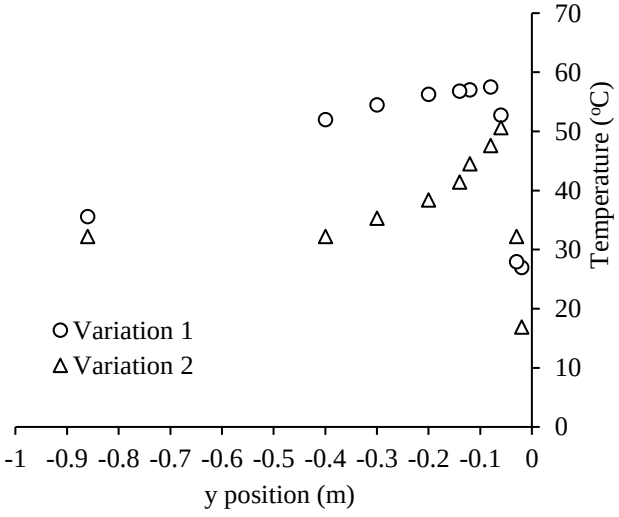

Fig. 8. Comparison of temperature distribution between variation 1 and 2

Vol.5 (No.1). 2023. pp. 16-25
Published online: April 1, 2023
ISSN: 2477-541X

right side of the drying chamber.

Fig. 8 shows the comparison of the chamber temperature distribution along the y direction between variations 1 and 2 that temperature variation 1 increased significantly more than variation 2. It implies that the quality of the mixture between the spray nozzle and the dry air is well mixed at variation 1. The material that receives the hot air is simultaneously and gradually degraded according to its distance from the drying heat source, i.e., at the top of the drying chamber. Air and materials will be separated in the cyclone chamber. High temperatures result in better heat transfer near the nozzles seen at nodes 3 and 4. The effect of a strong vortex will be better to promote drying near the spray so that it can be retained longer at nodes 3, 4, and 5. Particle agglomeration begins at point 3, and at the next node, product growth crystallizes. The high-velocity re-entrained particles from the unit indicate continuous flow; after that, the particle temperature becomes constant at node 10.

The novelty of this simulation is using a spray dryer machine with a combination of heating from the heater and exhaust heat from the condenser in the refrigeration system.

So, it is obvious that variation 1 is more recommended than variation 2. The limitation of this study lies in the number of inlets in the spray dryer, which is only one channel. Future research can be done with two or three drying air ducts that enter the drying chamber. So that there is a centrifugal effect that can collide with each other in the middle of the drying chamber and can minimize the occurrence of splashes of liquid material to the edge of the drying chamber. But of course, the numerical analysis will be more complex.

4. Conclusions

Contour and velocity vector simulations of both positions of the drying air inlet in the drying chamber show the tangential velocity of the drying airflow. Variation 1, which offers a more significant increase in the tangential velocity of the incoming air, will result in a greater increase in the evaporation rate as well in the spray dryer. Temperature variation 1 increased significantly compared to variation 2. It implies that the quality of the mixture between the spray nozzle and the dry air is well-mixed. However, getting further away from the heat source, temperature variations 1 and 2 lead to the same pattern: a decrease in temperature at node 10.

5. Acknowledgements

This study was conducted as part of a research project entitled "CFD simulation: Effect of dryer air inlet position on the spray dryer drying room to increase swirling flow effect," sponsored by Universitas Mercu Buana Research Center (Project No. 02-5/656/B-SPK/II/2021). The author thanks Mr. Fajar Anggara for his assistance in conducting this experiment and for his innovative ideas.

References

[1] Hussain, F., Jaskulski, M., Piatkowski, M., & Tsotsas, E. (2022). CFD simulation of agglomeration and coalescence in spray dryer. *Chemical Engineering Science*, *247*, 117064.

[2] Ali, M., Mahmud, T., Heggs, P. J., Ghadiri, M., Bayly, A., Ahmadian, H., & de Juan, L. M. (2015). CFD simulation of a counter-current spray drying tower with stochastic treatment of particle-wall collision. *Procedia engineering*, *102*, 1284-1294.

[3] Kosasih, E. A., & Ruhyat, N. (2016). Combination of electric air heater and refrigeration system to reduce energy consumption: A simulation of thermodynamic system. *International Journal of Technology*, *2*, 288-295.

[4] Schuck, P., Jeantet, R., Bhandari, B., Chen, X. D., Perrone, I. T., de Carvalho, A. F., ... & Kelly, P. (2016). Recent advances in spray drying relevant to the dairy industry: A comprehensive critical review. *Drying Technology*, *34*(15), 1773-1790.

[5] Cheow, W. S., & Hadinoto, K. (2010). Enhancing encapsulation efficiency of highly water-soluble antibiotic in poly (lactic-co-glycolic acid) nanoparticles: Modifications of standard nanoparticle preparation methods. *Colloids and Surfaces A: Physicochemical and Engineering Aspects*, *370*(1-3), 79-86.

[6] Masters, K. (1991). *Spray Drying Handbook*, Longman Scientific & Technical.

[7] Bhandari, B. R., Datta, N., & Howes, T. (1997). Problems associated with spray drying of sugar-rich foods. *Drying technology*, *15*(2), 671-684.

[8] Masters, K. (1994). Scale-up of spray dryers. *Drying technology*, *12*(1-2), 235-257.

[9] Chegini, G. R., & Ghobadian, B. (2005). Effect of spray-drying conditions on physical properties of orange juice powder. *Drying technology*, *23*(3), 657-668.

[10] Desobry, S. A., Netto, F. M., & Labuza, T. P. (1997). Comparison of spray-drying, drum-drying and freeze-drying for β-carotene encapsulation and preservation. *Journal of Food Science*, *62*(6), 1158-1162.

Vol.5 (No.1). 2023. pp. 16-25
Published online: April 1, 2023
ISSN: 2477-541X

[11] Al-Asheh, S., Jumah, R., Banat, F., & Hammad, S. (2003). The use of experimental factorial design for analysing the effect of spray dryer operating variables on the production of tomato powder. *Food and bioproducts processing*, *81*(2), 81-88.

[12] Abadio, F. D. B., Domingues, A. M., Borges, S. V., & Oliveira, V. M. (2004). Physical properties of powdered pineapple (Ananas comosus) juice––effect of malt dextrin concentration and atomization speed. *Journal of Food Engineering*, *64*(3), 285-287.

[13] Nath, S., & Satpathy, G. R. (1998). A systematic approach for investigation of spray drying processes. *Drying technology*, *16*(6), 1173-1193.

[14] Patil, V., Chauhan, A. K., & Singh, R. P. (2014). Optimization of the spray-drying process for developing guava powder using response surface methodology. *Powder Technology*, *253*, 230-236.

[15] Jaskulski, M., Wawrzyniak, P., & Zbiciński, I. (2015). CFD model of particle agglomeration in spray drying. *Drying technology*, *33*(15-16), 1971-1980.

[16] Roustapour, O. R., Hosseinalipour, M., Ghobadian, B., Mohaghegh, F., & Azad, N. M. (2009). A proposed numerical–experimental method for drying kinetics in a spray dryer. *Journal of Food Engineering*, *90*(1), 20-26.

[17] Huang, L., & Mujumdar, A. S. (2006). Numerical study of two-stage horizontal spray dryers using computational fluid dynamics. *Drying Technology*, *24*(6), 727-733.

[18] Sudarma, A. F. & Morsy, M. (2017). RANS numerical simulation of lean premixed bluff body stabilized combustor: Comparison of turbulence models. *Journal of Thermal Engineering*, *3*(6), 1561-1573.

[19] Tan, L. W., Ibrahim, M. N., Kamil, R., & Taip, F. S. (2011). Empirical modeling for spray drying process of sticky and non-sticky products. *Procedia Food Science*, *1*, 690-697.